SUPPLEMENTARY INFORMATION

AN EXCITABLE GENE REGULATORY CIRCUIT INDUCES TRANSIENT CELLULAR DIFFERENTIATION

Gürol M. Süel,[1] Jordi Garcia-Ojalvo,[2] Louisa L. Liberman,[1] and Michael B. Elowitz[1]

[1]*Division of Biology and Department of Applied Physics, California Institute of Technology, Pasadena, CA 91125*

[2]*Departament de Física i Enginyeria Nuclear, Universitat Politècnica de Catalunya, Colom 11, 08222 Terrassa, Spain*

Contents

S1. MATERIALS AND METHODS

S1.A. Cloning and strain construction

Polymerase Chain Reaction (PCR) was utilized to amplify native P_{comK}, P_{comG} and P_{comS} promoters as well as *comS* from the wild type *B. subtilis* PY79 strain (kind gift from Jonathan Dworkin) using Pfx DNA polymerase (Invitrogen). For each of the promoters, we amplified the entire sequence between the ribosome binding site and the preceeding structural gene. These products were then used to generate promoter-*yfp/cfp* (*yfp* and *cfp* were obtained from pDH5 plasmid and University of Washington Yeast Resource Center, respectively) and P_{comG}-*comS* fusions. All of these constructs were obtained using standard fusion PCR techniques with Pfx and cloned into *B. subtilis* integration vectors. We used *BamH1* and *EcoR1* sites within the pDL30 (kind gift from Jonathan Dworkin), pPyr-Cm, pSac-Cm (constructed by R. Middleton and obtained from the *B. subtilis* Stock Center) integration vectors for cloning. Standard *B. subtilis* transformation protocols were followed to transform *B. subtilis* strain PY79 with these plasmids. Integration of constructs into the chromosome were verified by PCR and sequencing. We incorporated several terminator sequences around the constructs to prevent read through transcription from chromosomal promoters near the integration sites. Furthermore, we observed no dependence of expression dynamics on integration site or orientation of the constructs with respect to the chromosome.

S1.B. Preparation of cells for microscopy

Cells were grown at 37°C in Luria Broth (LB) to an O.D. of 1.8 and resuspended in 0.5 volume of resuspension medium (RM) [S1] supplemented with 0.02% glucose. After 1.5 hour incubation at 37°C, cells were diluted 10-fold in RM and applied at appropriate densities (5-10 cells per field of view) onto a 1.5% low melting agarose pad made with RM and placed into a coverslip-bottom Willco dish. Willco dishes were sealed with parafilm to reduce evaporation from the agarose pads during the course of movie making. This protocol is optimized for time-lapse microscopy. RM reduces the growth rate of microcolonies on agarose and leads to sporulation. As a result, overgrowth of cells in the field of view is prevented, allowing the tracking of individual cell lineages for longer periods of time.

S1.C. Time-lapse microscopy

Growth of microcolonies was observed with fluorescence time-lapse microscopy at 37°C (temperature controlled chamber) using an Olympus IX-81 inverted microscope with a motorized stage (ASI). A Lambda-LS light source (Sutter Instruments) was used to excite fluorescence. Images were obtained with a Hamamatsu ORCA-ER camera. Custom written Visual Basic software was used to control the microscope and related equipment during the movie acquisition. Images were acquired every 20 minutes. Median cell cycle division times (excluding competence events) under these conditions are ∼200 minutes. We tested the effect of light exposure on cells and determined

that unfiltered exposure to the excitation light source lead to phototoxicity that resulted in the lysis of cells. We therefore used a combination of ultraviolet/infrared and neutral density filters to prevent phototoxicity. Even with these filters, acquisition rates faster than seven minutes per frame also resulted in phototoxicity-induced lysis. A typical dose response to light was determined (data not shown) by varying acquisition rates and counting lysis events. Frame rate (20 minutes) was chosen to minimize or eliminate such effects.

S1.D. Data analysis

Time-lapse microscopy movies were analyzed with the Matlab based custom made "schnitzcell" software package and other custom software [S2].

S1.E. Analysis in different growth conditions

Competence has previously been characterized in a specific medium [S3]. To determine the generality of our results we grew the P_{comG}-*cfp* / P_{comS}-*yfp* reporter strain in both RM media and traditional competence media (CM) [S3]. Cells grown in RM and CM were analyzed using fluorescence microscopy as described above. Microscopy images were quantified using Matlab-based custom written software, also described above. The resulting data are shown in Fig. S10 below. These data show that ComS is similarly repressed in both media.

S2. ANALYSIS OF THE DYNAMICAL MODEL

S2.A. Basic model of the competence module

The gene regulatory network underlying the development of competence in *B. subtilis* is shown in Fig. S1. On the basis of the assumptions made in the main text, we have concentrated on the simple module shown in Fig. 1 (main text). As discussed below, we have analyzed several variant models of this module and show that qualitatively similar results are obtained for all.

The interaction map within the core competent module (Fig. 1, main text) contains the following ingredients:

- ComK activates itself via a transcriptional autoregulatory positive feedback loop.
- ComK inhibits ComS expression via indirect transcriptional repression.
- MecA inhibits ComK via enzymatic degradation.
- The latter reaction is inhibited by ComS via competitive binding.

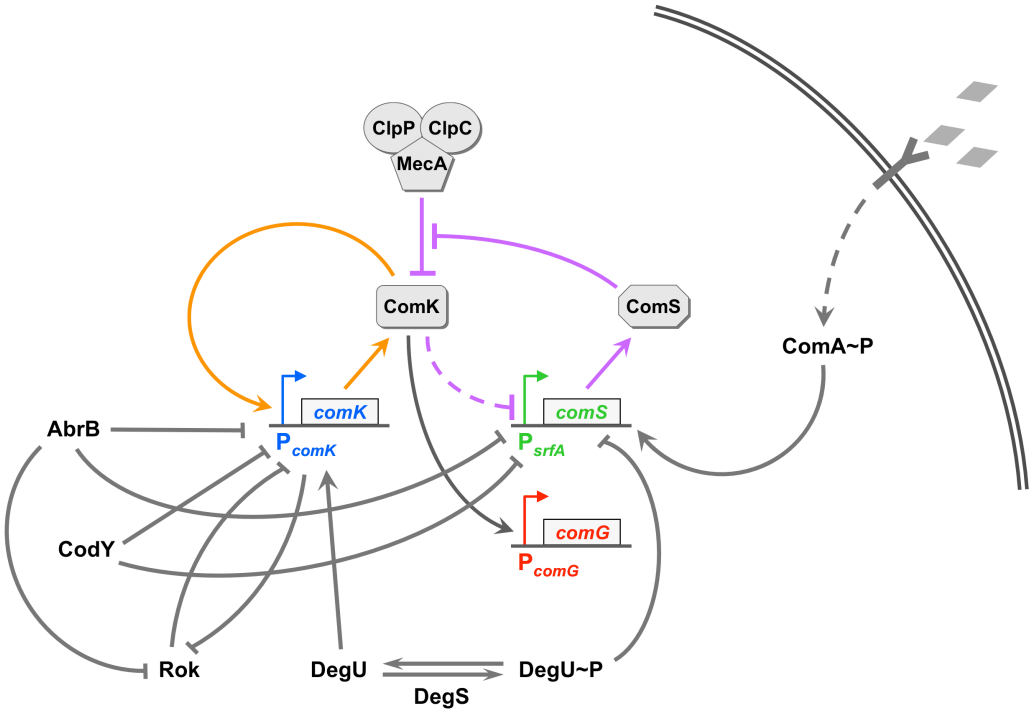

FIG. S1: Comprehensive map of molecular interactions within the *B. subtilis* competence network. Shown are selected genes and proteins within one link of the MeKS module. Transcriptional inputs to PcomK influence the fraction of competent cells in the population. AbrB is a global regulator that affects both sporulation and competence [S4]. CodY activity depends on intracellular GTP levels [S5]. Additionally, DegU/S is a two component system that also influences other stress responses such as swarming. The simplified MeKS model neglects these inputs because they do not appear to strongly influence the behavior of system once competence is initiated (see Fig. 2 in the main text). However, more detailed studies will be necessary to understand their role in the complete system.

ComK inhibits ComS expression by an effective Hill repression function [S2]. The enzymatic degradation reactions are assumed to be of the standard Michaelis-Menten form:

$$\begin{aligned} \text{MecA} + \text{ComK} &\overset{\gamma_{\pm a}}{\rightleftharpoons} \text{MecA-ComK} \overset{\gamma_1}{\rightarrow} \text{MecA} \\ \text{MecA} + \text{ComS} &\overset{\gamma_{\pm b}}{\rightleftharpoons} \text{MecA-ComS} \overset{\gamma_2}{\rightarrow} \text{MecA} \end{aligned}$$

Denoting by K and S the protein concentrations of ComK and ComS, respectively, and by M_f, M_K and M_S the concentrations of free MecA and of the complexes MecA-ComK and MecA-ComS, respectively, the dynamics of the network shown in Fig. 1 can be described by the following rate

equations:

$$\frac{dK}{dt} = \alpha_k + \frac{\beta_k K^n}{k_k^n + K^n} - \gamma_a M_f K + \gamma_{-a} M_K \tag{S1}$$

$$\frac{dS}{dt} = \frac{\beta_s}{1 + (K/k_s)^p} - \gamma_b M_f S + \gamma_{-b} M_S \tag{S2}$$

$$\frac{dM_K}{dt} = -(\gamma_{-a} + \gamma_1) M_K + \gamma_a M_f K \tag{S3}$$

$$\frac{dM_S}{dt} = -(\gamma_{-b} + \gamma_2) M_K + \gamma_b M_f K \tag{S4}$$

The meaning of the parameters are given in Table S1. In particular, the expression rate of ComS, β_s, can be expected to increase with nutrient limitation, since ComS expression is activated by starvation and cell crowding via the upstream protein ComA (see Fig. S1) [S6]. A differential equation for M_f is not necessary because we assume that the total amount of MecA is conserved:

$$M_f + M_K + M_S = M_{\text{total}} = \text{constant} \tag{S5}$$

Parameter	**Description**	**Value**
α_k	Basal expression rate of ComK	0.0028 nM/s
β_k	Saturating expression rate of ComK positive feedback	0.049 nM/s
β_s	Unrepressed expression rate of ComS	0.057 nM/s
k_k	ComK concentration for half-maximal ComK activation	100 nM
k_s	ComK concentration for half-maximal ComS repression	110 nM
δ_k	Unrepressed degradation rate of ComK	0.0014 s^{-1}
δ_s	Unrepressed degradation rate of ComS	0.0014 s^{-1}
Γ_k	ComK concentration for half-maximal degradation	500 nM
Γ_s	ComS concentration for half-maximal degradation	50 nM
n	Hill coefficient of ComK positive feedback	2
p	Hill coefficient of ComS repression by ComK	5

TABLE S1: Parameters of the dynamical model. The actual values of the parameters are obtained from the dimensionless parameters given in Table S2.

Assuming that γ_1^{-1} and γ_2^{-1} are much smaller than any other time scale in the system, we can adiabatically eliminate M_K and M_S. Therefore, taking the derivatives in Eqs. (S3)-(S4) equal to zero, and using relation (S5) leads to the reduced model:

$$\frac{dK}{dt} = \alpha_k + \frac{\beta_k K^n}{k_k^n + K^n} - \frac{\delta_k K}{1 + \frac{K}{\Gamma_k} + \frac{S}{\Gamma_s}} \tag{S6}$$

$$\frac{dS}{dt} = \frac{\beta_s}{1 + (K/k_s)^p} - \frac{\delta_s S}{1 + \frac{K}{\Gamma_k} + \frac{S}{\Gamma_s}} \tag{S7}$$

where

$$\Gamma_k = \frac{\gamma_{-a} + \gamma_1}{\gamma_a}, \qquad \Gamma_s = \frac{\gamma_{-b} + \gamma_2}{\gamma_b} \tag{S8}$$

and

$$\delta_k = \frac{\gamma_1 M_{\text{total}}}{\Gamma_k}, \qquad \delta_s = \frac{\gamma_2 M_{\text{total}}}{\Gamma_s} \tag{S9}$$

We have further assumed, without loss of generality, that the degradation rates δ_k and δ_s are equal. In that way, rescaling time with these rates and the concentrations of ComK and ComS with Γ_k and Γ_s, respectively, we obtain the dimensionless model:

$$\frac{dK}{dt} = a_k + \frac{b_k K^n}{k_0^n + K^n} - \frac{K}{1 + K + S} \tag{S10}$$

$$\frac{dS}{dt} = \frac{b_s}{1 + (K/k_1)^p} - \frac{S}{1 + K + S}\,, \tag{S11}$$

where now t, K and S are now dimensionless variables, and the dimensionless parameters of the model are defined as shown in Table S2. Reduction of the model to a set of two coupled differential equations allows a phase-plane analysis of the system dynamics, as described in what follows.

S2.B. Phase diagram

We now examine the dynamical behavior of model (S10)-(S11)[1]. The values chosen for the dimensionless parameters of the model are given in Table S2. These quantities translate into the real biochemical values listed in Table S1, determined by choosing the time unit $\delta_k^{-1} = \delta_s^{-1}$ to fit the experimentally observed excursion times (around 20 hours), and from educated guesses of the concentrations Γ_k and Γ_s.

Figure S2 shows the phase diagram of the model in the b_k-b_s plane. The diagram plots the number of fixed points in color coding, with red corresponding to three fixed points and blue to only one. In the blue area below the red region, the only fixed point is the vegetative state (low ComK), whereas in the area above, it is the competent state (high ComK). For the parameters chosen, the competent state undergoes a supercritical Hopf bifurcation (H) whose location, as computed with the continuation software AUTO [S8], is plotted in purple in the phase diagram. The green lines represent saddle-node (SN) bifurcations.

Parameter	**Definition**	**Value**
a_k	$\alpha_k/(\delta_k\Gamma_k)$	0.004
b_k	$\beta_k/(\delta_k\Gamma_k)$	0.07
b_s	$\beta_s/(\delta_s\Gamma_s)$	0.82
k_0	k_k/Γ_k	0.2
k_1	k_s/Γ_k	0.222
n	–	2
p	–	5

TABLE S2: Parameter values of the dimensionless model

[1] For an excellent introduction to the nonlinear dynamics concepts that will be used in what follows, see Ref. [S7].

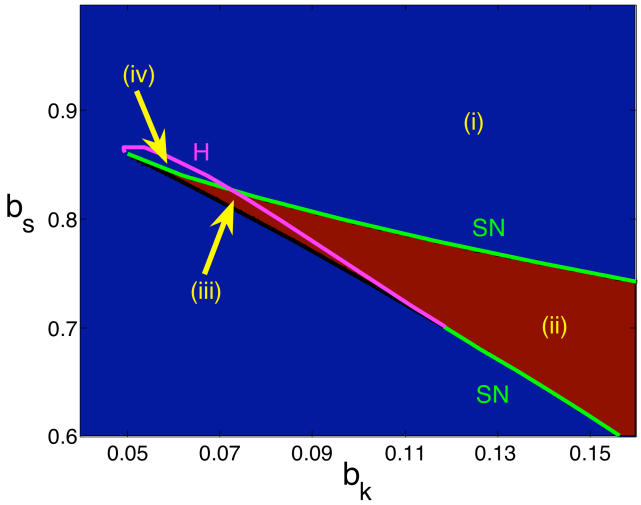

FIG. S2: Phase diagram showing the number of fixed points (in color coding) of model (S10)-(S11) and their instability boundaries. Blue represents a single fixed point and red corresponds to three fixed points. Yellow labels denote different regions described in the text. Parameter values are those of Table S2, except b_k and b_s, which are variable.

The different instability lines described above delineate four different regions, denoted by yellow numbers in Fig. S2, that can be described as follows:

(i) Monostability: only one fixed point exists, and it is stable. Typical phase-plane nullcline portraits are shown in Figs. S3A (vegetative state) and S3B (competent state).

(ii) Bistability: three fixed points exist, two of which are stable. The vegetative and the competent regimes coexist. A typical phase-plane nullcline portrait is shown in Fig. S3C. In that figure, the two stable fixed points are denoted by full circles, and the unstable saddle at intermediate values of ComK is represented by an empty circle.

(iii) Excitability: three fixed points exist, but only one of them is stable. The competent fixed point is an unstable spiral, and the mid-ComK fixed point remains a saddle point. Large enough perturbations will excite the system out of the vegetative state into the competence region, which can be interpreted as the area around the unstable spiral fixed point. A typical phase-plane nullcline portrait is shown in Fig. S3D.

(iv) Limit cycle oscillations: only one fixed point exists, but it is *unstable*. The system exhibits limit cycle oscillations between a mid-ComK and a high-ComK level.

The portion of SN boundary separating regions (iii) and (iv) corresponds to a homoclinic bifurcation. The limit cycle that exists in region (iv) disappears upon entering region (iii), after colliding with the newly born saddle point located at intermediate ComK levels (see Fig. S3C). In that way, within the excitability region no limit cycle exists, the only attractor being the vegetative fixed point.

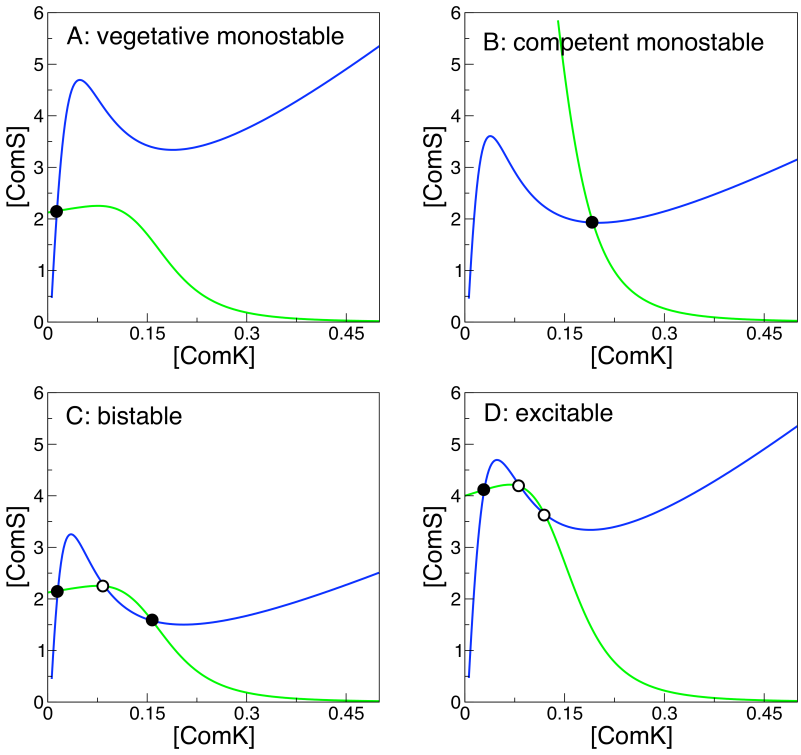

FIG. S3: Typical phase-plane nullcline portraits corresponding to regions (i)-(iii) in Fig. S2. The blue line corresponds to the ComK nullcline, and the green line to the ComS nullcline. Furthermore, the filled black dots denote stable fixed points, and the empty ones correspond to unstable fixed points. Parameter values are those of Table S2, except: (A) $b_k = 0.08$, $b_s = 0.68$, (B) $b_k = 0.12$, $b_s = 0.92$, (C) $b_k = 0.14$, $b_s = 0.68$, and (D) $b_k = 0.08$, $b_s = 0.8$.

S2.C. Exciting competence

Let us now concentrate on the excitable regime existing in region (iii) of the phase diagram shown in Fig. S2 (see also Fig. S3C). As mentioned earlier, a sufficiently large perturbation of the vegetative state will excite a large-amplitude excursion through the competence region in phase space. Stochasticity of gene regulation provides a rich source of such perturbations. We have considered three different possible sources of competence-triggering fluctuations:

1. Multiplicative noise acting parametrically on b_s:

$$\frac{dS}{dt} = \frac{b_s + \xi(t)}{1 + (K/k_1)^p} - \frac{S}{1 + K + S}$$

2. Additive noise acting on ComS promoter activity:

$$\frac{dS}{dt} = \frac{b_s}{1 + (K/k_1)^p} - \frac{S}{1 + K + S} + \xi(t)$$

3. Additive noise acting on ComK promoter activity:

$$\frac{dK}{dt} = a_k + \frac{b_k K^n}{k_0^n + K^n} - \frac{K}{1 + K + S} + \xi(t)$$

In all cases, we use a Gaussian noise with zero mean and an exponentially decaying correlation in time

$$\langle \xi(t)\xi(t')\rangle = \frac{D}{\tau_c}\exp\left(-\frac{|t-t'|}{\tau_c}\right)$$

This is the so-called Ornstein-Uhlenbeck noise. The choice of this type of correlation is motivated by recent studies in gene expression noise dynamics [S2]. The correlation time is taken to be roughly of the order of the cell-cycle duration. Noise with shorter correlation times also trigger competence and may be more compatible with sister cell results. We have checked that all three types of perturbations are able to trigger competence events in the system. Furthermore, we note that in the presence of time-correlated noise, competence events can also be excited outside (below) region (iii), when fluctuations take the cell transiently within that region. The values of the noise parameters used in this paper are $D = 0.01$ and $\tau_c = 3$, which correspond to a noise amplitude $\sqrt{D/\tau_c} = 0.058$ in dimensionless units. This value is approximately 7% of the full expression level of ComS, given by $b_s = 0.82$.

S2.D. Delayed repression of ComS by ComK

The excitable region (iii) shown in the phase diagram of Fig. S2 is rather small. This limitation is removed in the presence of time delay in the repression of ComS expression by ComK. This delay is expected given that this link is indirect. To incorporate the delay, we modify the model substituting Eq. (S11) by

$$\frac{dS}{dt} = \frac{b_s}{1+(K(t-\tau)/k_1)^p} - \frac{S}{1+K+S}\,, \tag{S12}$$

where τ is the delay time, measured in units of $1/\delta_k$.

The time delay has no effect on the stability of either the vegetative fixed point or the saddle at intermediate ComK levels, but does affect the competent fixed point, which is the only spiral point of the dynamics in this area of parameter space. A large enough delay destabilizes this fixed point, as shown schematically in Fig. S4. The result of this destabilization is that the size of region (iii) increases. Delays were previously shown to destabilize stable states in biological systems [S9].

The influence of the delay time on the position of the Hopf instability line is shown in Fig. S5A, as obtained with the continuation software DDE-BIFTOOL [S10]. For small delays the Hopf line moves upwards, so that the size of the region where the competent fixed point is unstable increases. This in turn increases the region of excitability, which is the portion of red area where that fixed point is unstable. For larger delays (e.g. $\tau = 1.08$, corresponding to a delay time of approximately 12 min, and shown by a yellow line in plot S5A) a second Hopf instability line comes from above. Collision between the two lines (see e.g. the green line corresponding to $\tau = 1.1$) increases substantially the region of instability of the competent fixed point, and for larger τ values that fixed point is unstable everywhere in the plotted region. This tendency is similar for smaller values of the Hill coefficient p, although the values of τ needed to destabilize the competent fixed point in that case are slightly larger (see Fig. S5B). These results show that excitability is a generic feature of this model in the presence of delay.

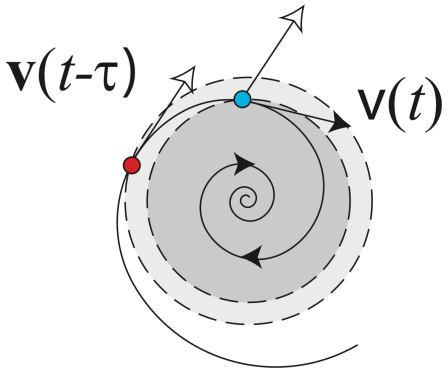

FIG. S4: Qualitative sketch showing the effect of time delay on the stability of a spiral fixed point. At a given time instant, the velocity vector to which the trajectory is tangential is the combination of the previous vector and a delayed one. For large enough delays, this combination begins to point outwards, destabilizing the spiral. Note that this heuristic argument holds close enough to the fixed point, so that a linearization of the dynamics is possible, and for time delays smaller than the characteristic period of the spiral point, even though destabilization occurs even in the absence of this latter requirement.

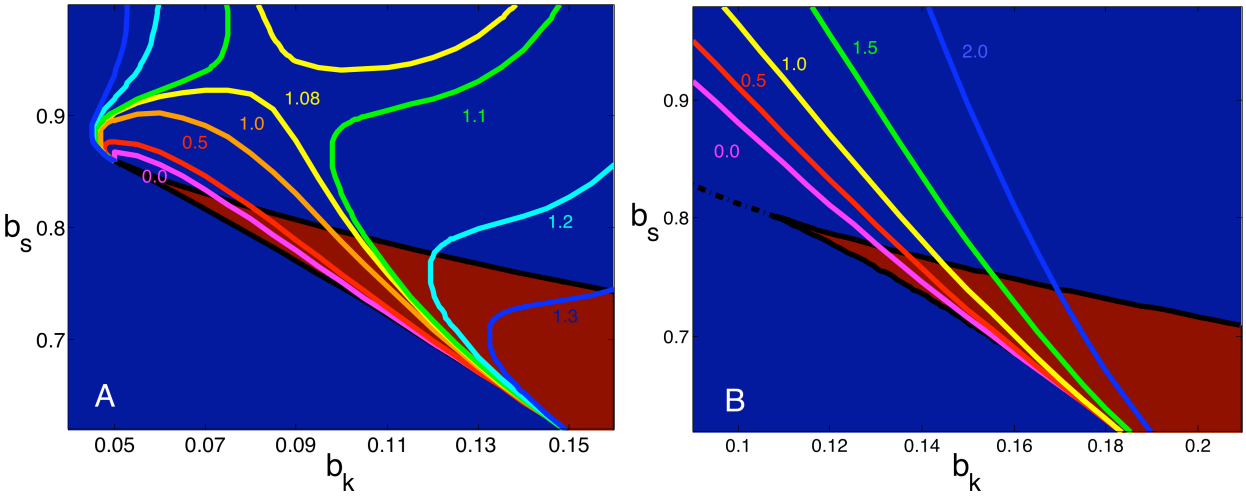

FIG. S5: Effect of increasing time delay on the position of the Hopf instability line (colored lines). The value of the delay time is shown next to each line, in units of $1/\delta_k \approx 12$ min. The solid black lines are the saddle-node bifurcation lines, and the dot-dashed black line in plot B represents a supercritical Hopf boundary which is generic for all values of the delay. Parameter values are those of Table S2, except $p = 2.5$ in plot B.

S2.E. Modeling the effect of feedback bypass

As described in the main text, a Feedback Bypass (FeBy) strain of *B. subtilis* was constructed in which a single chromosomal copy of the pure ComK promoter P_{comG} drives expression of ComS. This is modeled by introducing an extra term into the ComS equation (S11):

$$\frac{dS}{dt} = \frac{b_s}{1+(K/k_1)^p} + \frac{b_g K^n}{k_g^n + K^n} - \frac{S}{1+K+S}\,. \tag{S13}$$

In other words, ComK activates expression of ComS via a Hill function with the same cooperativity coefficient as the positive transcriptional feedback of ComK on itself. We also assume the same concentration value for half-maximal activation, $k_g = k_0 = 0.2$. Figure S6 shows the phase-plane portrait of the system for $b_g = 0.20$. The plot shows that trajectories now tend to the competent fixed point, which has been rendered stable by the feedback bypass link (and whose stability is much larger than that of the vegetative fixed point). This behavior may be compared with Fig. 5 (main text).

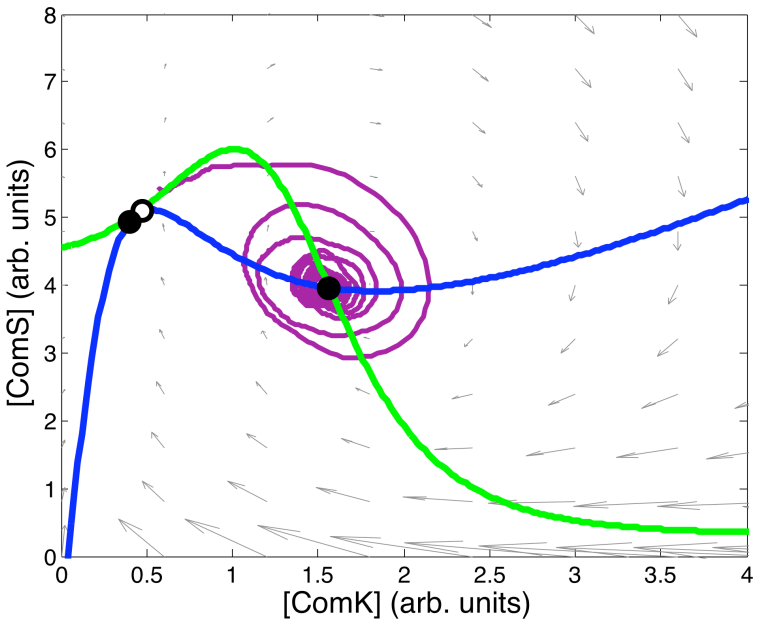

FIG. S6: Phase plane portrait of the feedback bypass system. The competent fixed point is now stable (rightmost full circle).

S3. COMPARING EXCURSION TIMES IN SISTER CELLS

In order to check whether competent sister cells are more likely to exhibit similar excursion times because they share initial conditions, we have statistically analyzed the difference between excursion times in sister cells and in the general cell population. The resulting cumulative histograms are plotted in Fig. S7. As can be seen, the two distributions are highly similar as determined by the Kolmogorov-Smirnov test ($p = 0.89$). Simulations of the MeKS model yield qualitatively similar results, as shown in Fig. S8 (compare with Fig. 3e, main text).

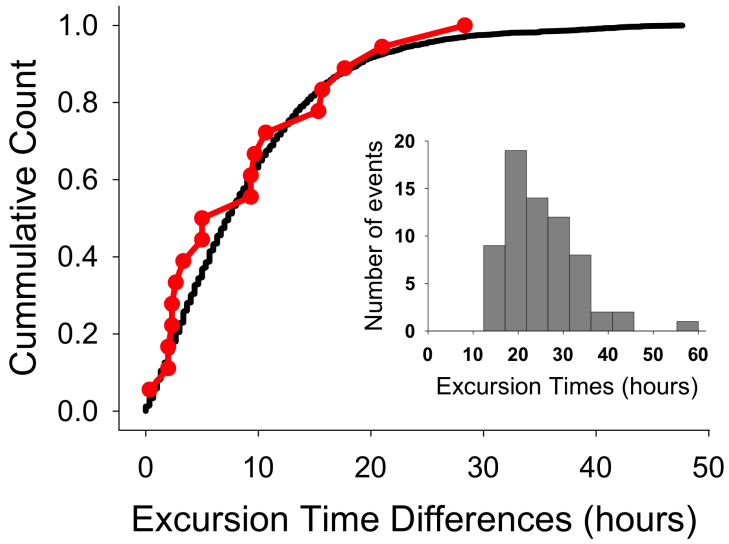

FIG. S7: Cumulative histograms of differences between excursion times as measured experimentally. Shown in black is the cumulative histogram of differences between all competence events recorded. In red, cumulative histogram of differences between sister cell competence events. The inset shows the histogram of excursion times for all the measured events.

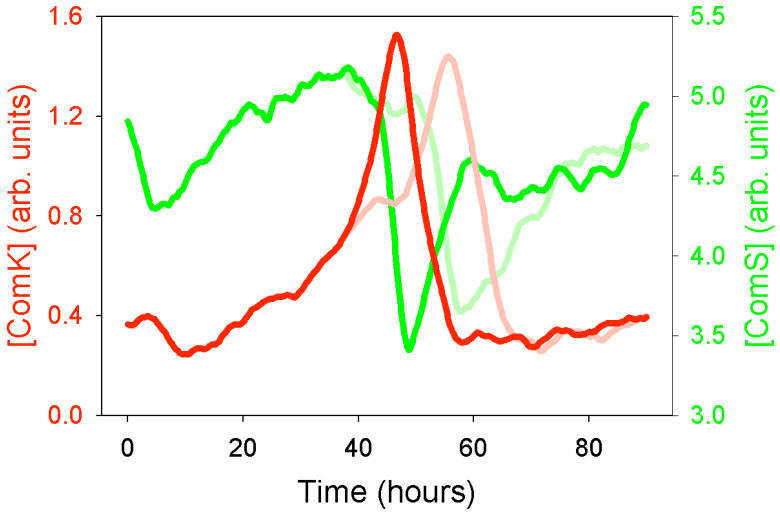

FIG. S8: Numerically simulated time traces of two sister cells undergoing competence. ComK traces are shown in shades of red and ComS in shades of green. Compare with Fig. 3e (main text).

S4. ADDITIONAL SUPPLEMENTARY FIGURES

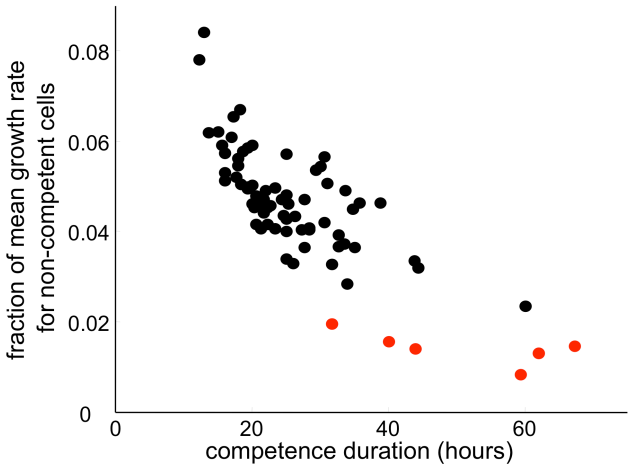

FIG. S9: **Competence retards cellular growth.** Shown in black (red) are single-cell competent events from the wild-type (FeBy) strain. Competence duration of FeBy cells is defined as the time between entry into competence and cell death due to phototoxicity. Growth rate refers to the mean logarithmic increase in total cell length per unit time during competence, normalized by the growth rate of non-competent cells. Note that compared to competent cells, non-competent cells have at least a ten-fold slower growth rate.

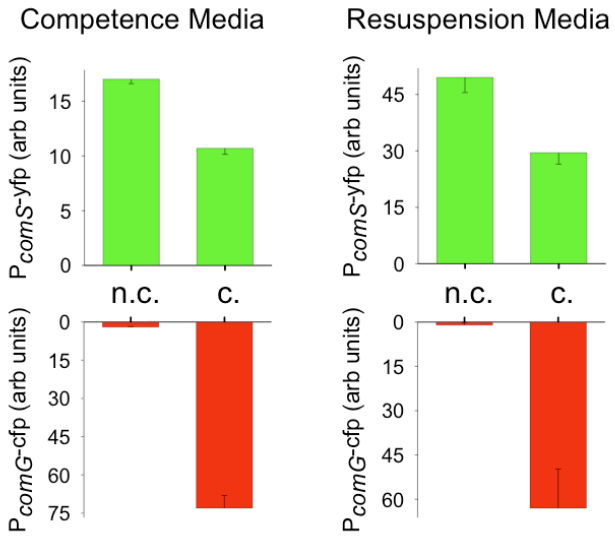

FIG. S10: **Comparing competence and resuspension media.** Shown are mean P$_{comS}$-*yfp* (green color) and P$_{comG}$-*cfp* (red color) expression in non-competent (n.c.) and competent (c) cells in competence and resuspension media. Note that the relative reduction in comS expression is the same (∼60%) in both media, despite a change in the absolute expression level. These data show that the repression of P$_{comS}$-*yfp* in competent cells is qualitatively similar in both RM and CM media.

[S1] Sterlini, J. M. & Mandelstam, J. Commitment to sporulation in *Bacillus subtilis* and its relationship to development of actinomycin resistance. Biochem J **113**, 29–37 (1969).

[S2] Rosenfeld, N., Young, J. W., Alon, U., Swain, P. S. & Elowitz, M. B. Gene regulation at the single-cell level. Science **307**, 1962–5 (2005).

[S3] Dubnau, D., Davidoff-Abelson, R. & Smith, I. Transformation and transduction in *Bacillus subtilis*: evidence for separate modes of recombinant formation. J Mol Biol **45**, 155–79 (1969).

[S4] Grossman, A. D. Genetic networks controlling the initiation of sporulation and the development of genetic competence in *Bacillus subtilis*. Annu Rev Genet **29**, 477-508 (1995).

[S5] Hamoen, L. W., Venema, G. & Kuipers, O. P. Controlling competence in *Bacillus subtilis*: shared use of regulators. Microbiology **149**, 9-17 (2003).

[S6] Lazazzera, B. A. Quorum sensing and starvation: signals for entry into stationary phase. Curr Opin Microbiol **3**, 177–182 (2000).

[S7] Strogatz, S. H., *Nonlinear Dynamics and Chaos* (Addison-Wesley, Reading, 1994).

[S8] http://indy.cs.concordia.ca/auto/

[S9] Lewis, J. Autoinhibition with transcriptional delay: a simple mechanism for the zebrafish somitogenesis oscillator. Curr Biol **13**, 1398-408 (2003).

[S10] Engelborghs, K., Luzyanina, T. & Roose, D. Numerical bifurcation analysis of delay differential equations using DDE-BIFTOOL. ACM Trans Math Softw **28**, 1–21 (2002).